Supplement of Biogeosciences, 22, 7137–7148, 2025 https://doi.org/10.5194/bg-22-7137-2025-supplement © Author(s) 2025. CC BY 4.0 License.





Supplement of

Technical note: In situ photosynthesis-irradiance curve determination in peatlands with a modulated-light skirt-chamber

Frederic Thalasso et al.

Correspondence to: Frederic Thalasso (thalasso@cinvestav.mx) and Julio A. Salas-Rabaza (jsalasrab@gmail.com)

The copyright of individual parts of the supplement might differ from the article licence.

S1. Chamber design and mass balance

The new modulated-light skirt-chamber was manufactured using 3D printing with thermoplastic polyurethane and consists of two sections (Figure 1). The first section is a ring-shaped base with an outer diameter of 320 mm and an inner diameter of 240 mm. This base is designed to be placed on the ground, with the plastic skirt glued to its upper surface. The base can also accommodate a steel chain placed above the plastic skirt to improve sealing with the ground. Along the inner perimeter of the base, a 5×5 mm groove allows the chamber (second section) to be positioned hermetically using silicone grease for sealing. The chamber is an oblique cylinder cut at a 40° angle from the horizontal, with a minimum height of 40 mm, a maximum height of 250 mm, an internal diameter of 240 mm, and a thickness of 15 mm. This design, combined with its orientability, enhances direct sunlight exposure for most of the day, even at relatively high latitudes where sun inclination is low. The internal surface of the chamber is covered with a reflective film (Q-BICS, Mexico) to ensure maximum light dispersion. Around the oblique cut, a 10×10 mm support ledge runs along the entire perimeter, positioned just 10 mm below the cut edge, to support an oval window made of 9 mm-thick commercial glass window, which is sealed with silicone. Within the chamber, two light/temperature data loggers are placed at ground level to measure light intensity. On the higher side of the chamber, a 180×40 mm opening leads to a rectangular extension housing a battery-operated fan, facilitating air circulation within the chamber. This design prevents the creation of shadows from the electric fan and optimizes light distribution over the entire ground surface. Inlet and outlet ports, positioned on opposite sides of the frame, are connected in recirculation mode to an UGGA (Los Gatos Inc., ABB, USA), which continuously measures CH₄ and CO₂ concentrations at 1 Hz. In this study, we focus solely on CO₂ emissions, although CH₄ concentrations are measured when used as a tracer gas to determine the gas residence time within the chamber, as described in section 2.2.

The concept of the chamber is the absence of a collar penetrating the ground, thus minimizing disturbance and reducing deployment time, but leading to imperfect sealing at the ground-chamber interface, allowing for gas exchange between the atmosphere and the chamber. Under these conditions, the mass balance of the chamber is as follows:

$$\frac{dC_{C,CO2}}{dt} = CO_2 flux + input caused by leaks - output caused by leaks$$
 (S1)

$$\frac{dC_{C,CO2}}{dt} = F_{CO2} \cdot \frac{A_C}{V_C} + \frac{Q_L}{V_C} \cdot C_{L,CO2} - \frac{Q_L}{V_C} \cdot C_{C,CO2}$$
(S2)

where $C_{C,CO2}$ is the CO₂ concentration within the chamber (µmol m⁻³), F_{CO2} is the CO₂ flux captured by the chamber (µmol m⁻² s⁻¹), A_C is the area of the chamber in contact with the ground (m²), V_C is the chamber volume (m⁻³), Q_L is the leak flow rate to/from the chamber (m³ s⁻¹), and $C_{L,CO2}$ is the CO₂ concentration at ground level outside the chamber, entering with the leaks (µmol m⁻³).

Given that Q_L/V_C is the dilution rate caused by leaks and is the inverse of the gas residence time within the chamber (θ_C, s) , Equation S2 can be rewritten as follows:

$$\frac{dC_{CO2}}{dt} = F_{CO2} \cdot \frac{A_C}{V_C} + \frac{Q_L}{V_C} \cdot \left(C_{L,CO2} - C_{C,CO2} \right) = F_{CO2} \cdot \frac{A_C}{V_C} + \frac{\left(C_{L,CO2} - C_{C,CO2} \right)}{\theta_C}$$
 (S3; 1)

In addition to Equation S3, like most gas analyzers, the UGGA includes a cavity where the gas pumped out from the chamber is measured, causing measurement delays. This introduces a slight difference between the gas concentration measured by the analyzer and the actual concentration within the chamber. To solve that aspect, the mass balance of the analyzer's cavity can be described as follows:

$$\frac{dC_{D,CO2}}{dt} = \frac{Q_D}{V_D} \cdot C_{C,CO2} - \frac{Q_D}{V_D} \cdot C_{D,CO2} = \frac{(C_{C,CO2} - C_{D,CO2})}{\theta_D}$$
(S4)

where $C_{D,CO2}$ is the CO₂ concentration measured (within the detector; μ mol m⁻³), Q_D is the flow rate to/from the detector (m³ s⁻¹), V_D is the detector's cavity volume (m³), and θ_D is the gas residence time within the detector's cavity.

Equation S4 can be rewritten to obtain the actual CO₂ concentration, as follows:

$$C_{C,CO2} = \frac{dC_{D,CO2}}{dt} \cdot \theta_D + C_{D,CO2}$$
 (S5)

By combining Equations S3 and S5, we obtain:

$$F_{CO2} = \left(\frac{dC_{C,CO2}}{dt} - \frac{(C_{L,CO2} - C_{C,CO2})}{\theta_C}\right) \cdot \frac{V_C}{A_C}$$
(S6)

In which $C_{C,CO2}$ is replaced by Equation S5.

S2. Determination of the chamber residence time (θ_C)

Resolving Equation S6 requires the determination of θ_C . The strategy included the creation of a transient state of the gas concentration, using CH₄ as a tracer gas. CH₄ was chosen, because it is detected by the UGGA and does not interfere with F_{CO2} measurements. Thus, the transient state and the determination of θ_C can be done during flux measurement. In practice, a pulse of CH₄ was injected into the chamber. After the CH₄ pulse injection, the CH₄ concentration within the chamber ($C_{C,CH4}$) is artificially increased and then tends to decrease back to a steady-state concentration at which the chamber is under equilibrium with the environment. This transient decrease of $C_{C,CH4}$ at any time, can be described by the following mass balance (similar to Equation S1,2):

$$\frac{dC_{C,CH4}}{dt} = CH_4 flux + input caused by leaks - output caused by leaks$$
 (S7)

$$\frac{dC_{C,CH4}}{dt} = F_{CH4} \cdot \frac{A_C}{V_C} + \frac{Q_L}{V_C} \cdot \left(C_{L,CH4} - C_{C,CH4} \right) = F_{CH4} \cdot \frac{A_C}{V_C} + \frac{\left(C_{L,CH4} - C_{C,CH4} \right)}{\theta_C}$$
 (S8)

In Equations S7 and S8 the variables are defined as follows: $C_{C,CH4}$ represents the CH₄ concentration inside the chamber (μ mol m⁻³); F_{CH4} denotes the CH₄ flux from the ecosystem (μ mol m⁻² s⁻¹); A_C represents the area of the chamber in contact with the ground (m²); V_C represents the chamber volume (m³); Q_L indicates the flowrate of gas exchange between the chamber and the

exterior due to leaks (m³ s⁻¹); and $C_{L,CH4}$ signifies the gas concentration at ground level outside the chamber (to be considered for leaks; μ mol m⁻³). The term Q_L/V_C is the dilution rate caused by the gas exchange between the chamber and the environment due to leak, which is the inverse of the mean residence time of the chamber (θ_C).

Under steady state, i.e. gas concentration not changing over time, Equation S8 would become:

$$0 = F_{CH4} \cdot \frac{A_C}{V_C} + \frac{(C_{L,CH4} - C_{C,CH4}^*)}{\theta_C}$$
 (S9)

Where $C_{C,CH4}^*$ is the concentration within the chamber that would be observed under steady state, i.e. constant. Under these conditions, Equation S9 can be reorganized as:

$$F_{CH4} \cdot \frac{A_C}{V_C} = -\frac{(C_{L,CH4} - C_{C,CH4}^*)}{\theta_C}$$
 (S10)

By combining Equations S8 and S10, we can write:

$$\frac{dC_{C,CH4}}{dt} = \frac{(C_{L,CH4} - C_{C,CH4})}{\theta_C} - \frac{(C_{L,CH4} - C_{C,CH4}^*)}{\theta_C} = \frac{C_{C,CH4}^* - C_{C,CH4}}{\theta_C}$$
(S11)

By variable separation and integration S11 can be written:

$$\int_0^t \frac{d(C_{C,CH4}^* - C_{C,CH4})}{(C_{C,CH4}^* - C_{C,CH4})} = -\int_0^t \frac{dt}{\theta_C}$$
 (S12)

$$ln\frac{(c_{C,CH4}^* - c_{C,CH4})_t}{(c_{C,CH4}^* - c_{C,CH4})_0} = -t/\theta_C$$
(S13)

$$\frac{C_{C,CH4}^* - C_{C,CH4,t}}{C_{C,CH4,0}^* - C_{C,CH4,0}} = e^{-t/\theta c}$$
(S14)

And finally:

$$C_{C,CH4}(t) = C_{C,CH4}^* - (C_{C,CH4}^* - C_{C,CH4,0}) \cdot e^{-t/\theta_C}$$
(S15)

It is important to note that for θ_C determination, any section of $C_{C,CH4}$ is valid, regardless of the initial and final $C_{C,CH4}$ values. A corollary of this is that the mass of CH₄ injected into the chamber is unimportant, as long as it is detectable. The selected section of $C_{C,CH4}$ was used to calibrate Equation S14, with θ_C and $C_{SS,CH4}$ as adjustment parameters and through the minimization of the Root Mean Square Error.

S3. Determination of the detector's cavity residence time (θ_D)

For the determination of θ_D , the same strategy and Equation S14 were used, except that θ_D substitutes θ_C and that a step increase of $C_{C,CH4}$ at the detector inflow was used (no chamber)

instead of a pulse concentration. Also, this determination was conducted in the laboratory, as θ_D is a detector parameter not changing over time.

Table S1: Percentage of light transmittance for the different fabrics used, as measured in the field under natural light conditions. Of the 11 fabrics tested, we progressively selected 6 that provided reliable data, which are marked with an asterisk.

Fabric	% transmittance	SD
None *	100.0%	-
1	85.2%	12.3%
2	57.4%	21.9%
3 *	51.1%	19.2%
4 *	35.9%	13.4%
5 *	22.3%	2.3%
6	21.2%	10.7%
7 *	15.5%	3.2%
8	12.7%	5.8%
9	5.0%	1.7%
10	1.1%	0.1%
11 *	0.4%	0.1%

Table S2: Site characteristics showing the dominant plant species and their relative cover (%) at each measurement location. Type of relief refers to the microtopographic position: hollow, hummock, or transition. Transition refers to the sloping areas between hollows and hummocks.

Site	Dominant species (% cover)	Type of relief
1	Tetroncium magellanicum (99.6)	Hollow
2	Tetroncium magellanicum (66.3)	Hollow
3	Tetroncium magellanicum (95.8)	Hollow
4	Tetroncium magellanicum (50.9)	Hummock
5	Ericaceae (93.9)	Hummock
2	Tetroncium magellanicum (66.3)	Hollow
7	Sphagnum magellanicum (78.3)	Hummock
8	Sphagnum magellanicum (65.4)	Hummock
9	Ericaceae (59.7)	Transition
10	Ericaceae (95.8)	Transition
11	Sphagnum magellanicum (50.7)	Hummock
12	Tetroncium magellanicum (95.8)	Hollow
13	Nothofagus antarctica (46.3)	Hummock
14	Lichens (79.5)	Hummock
15	Ericaceae (51.5)	Hollow
16	Ericaceae (51.5)	Hollow
17	Sphagnum magellanicum (90.2)	Hummock
18	Tetroncium magellanicum (80.3)	Transition
19	Sphagnum magellanicum (50.0)	Hummock
20	Ericaceae (100.0)	Hummock
21	Sphagnum magellanicum (100.0)	Hummock
22	Bare peat (64.6)	Hollow
23	Ericaceae (97.7)	Hummock
24	Ericaceae (88.1)	Hummock
25	Ericaceae (77.6)	Transition
26	Bare peat (76.6)	Hollow
_27	Ericaceae (47.9)	Hollow

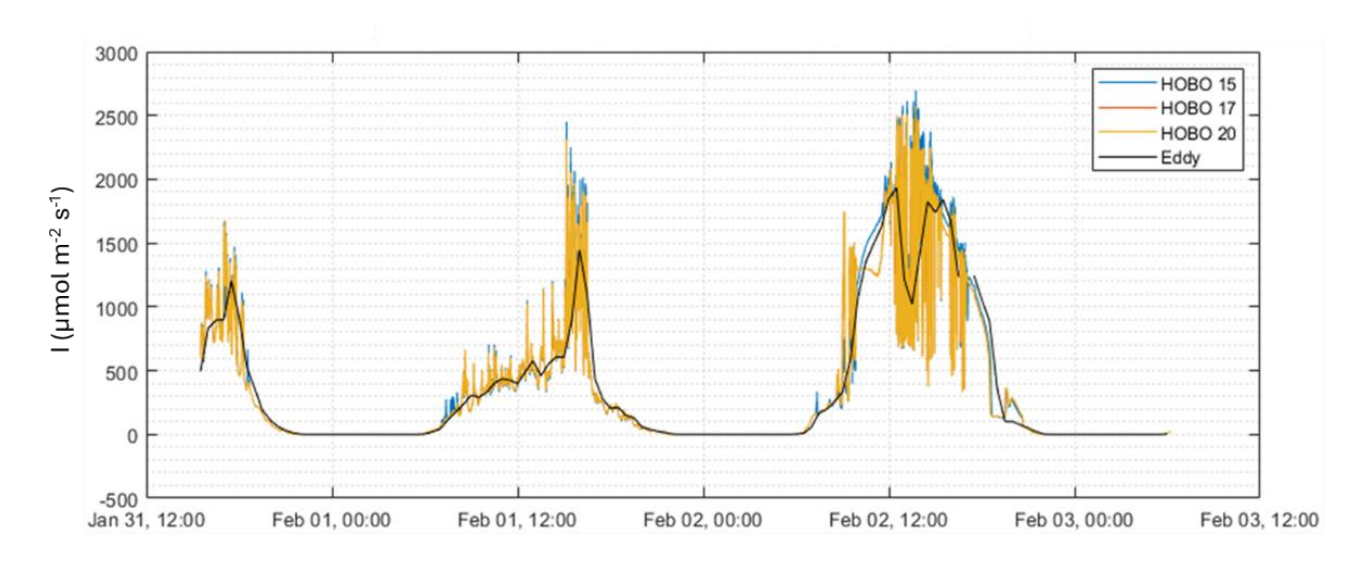


Figure S1. Irradiance measurements obtained during a 60 h field deployment using one PAR quantum sensor (LI-190R, LI-COR, USA) and three HOBO light/temperature data loggers (MX2202, HOBO, USA). HOBO light data (lux) were converted to PAR (μ mol m⁻² s⁻¹) using the best-fit relationship PAR = 0.0201 × lux, with a standard deviation of standard deviation of 0.0002 and a mean error of -4.3 μ mol m⁻² s⁻¹ relative to the LI-COR reference sensor.

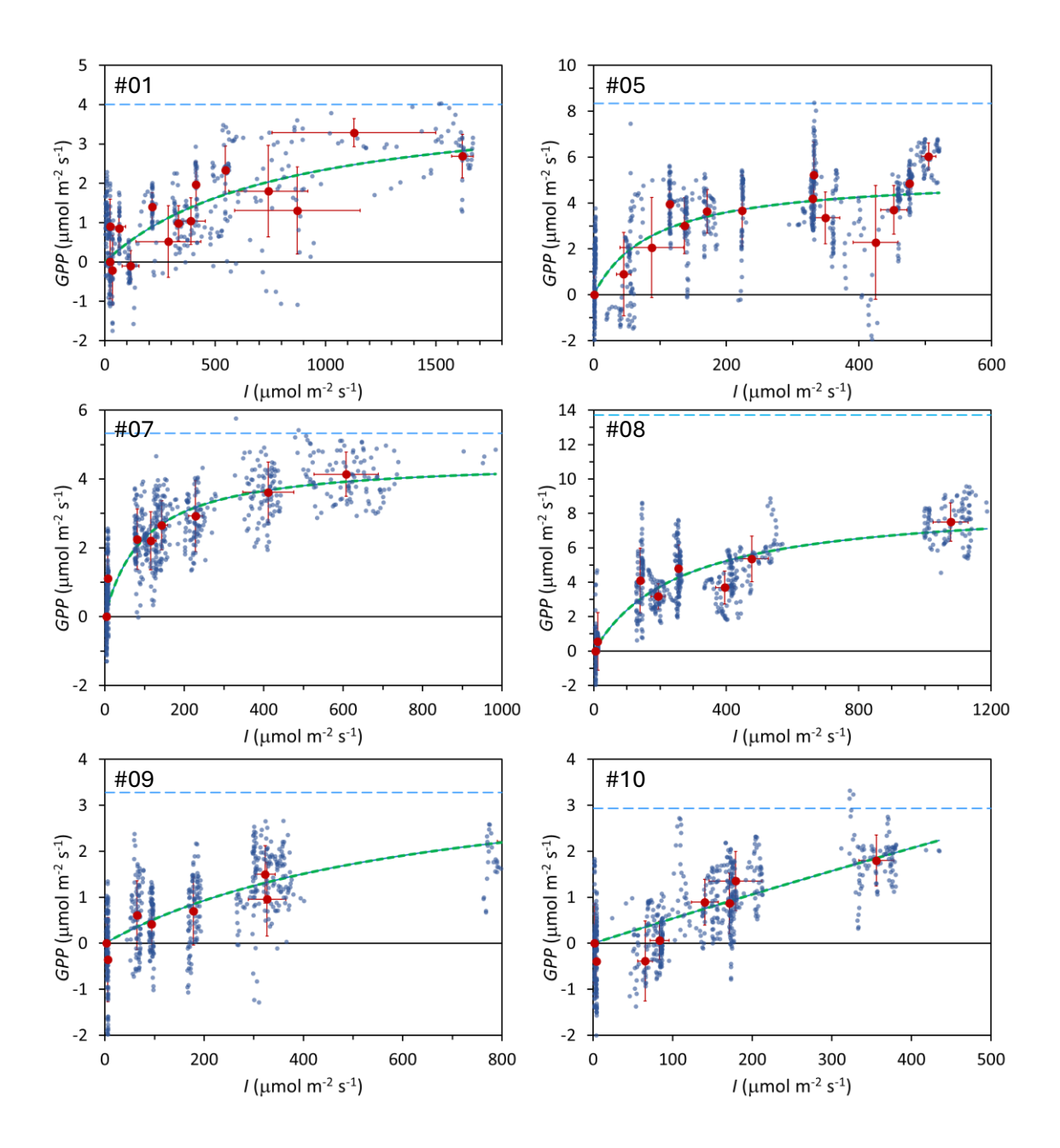


Figure S2 (1/2): Photosynthesis–Irradiance (PI) curves observed at 20 locations in a subantarctic peatland bog, measured in situ using the modulated-light skirt-chamber. Small blue points: individual measurements (500–900 data points per location). Large dark-red points: mean values of data clusters collected under each irradiance level, corresponding to each fabric screen used. Error bars on the dark-red points show one standard deviation. Thick green dotted line: Monod model fit; thin blue continuous line: Bernard–Rémond model fit; light blue dashed line: respiration (R_{eco}), expressed in the same units as GPP. Numbers in the upper left corner reference the experiment numbers listed in Table 1, where model parameters and statistics are provided.

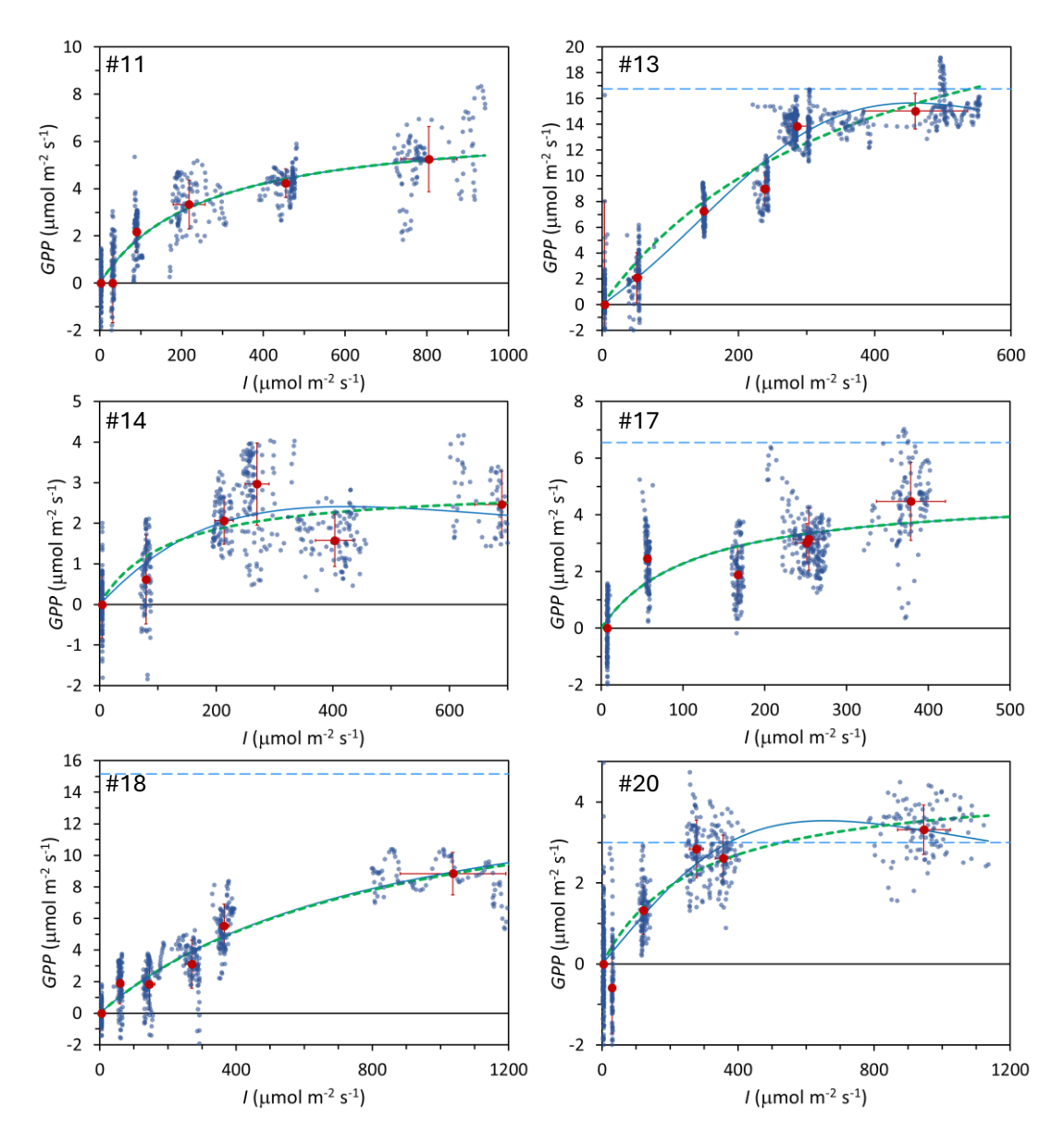


Figure S2 (2/2): Photosynthesis–Irradiance (PI) curves observed at 20 locations in a subantarctic peatland bog, measured in situ using the modulated-light skirt-chamber. Small blue points: individual measurements (500–900 data points per location). Large dark-red points: mean values of data clusters collected under each irradiance level, corresponding to each fabric screen used. Error bars on the dark-red points show one standard deviation. Thick green dotted line: Monod model fit; thin blue continuous line: Bernard–Rémond model fit; light blue dashed line: respiration (R_{eco}), expressed in the same units as GPP. Numbers in the upper left corner reference the experiment numbers listed in Table 1, where model parameters and statistics are provided.

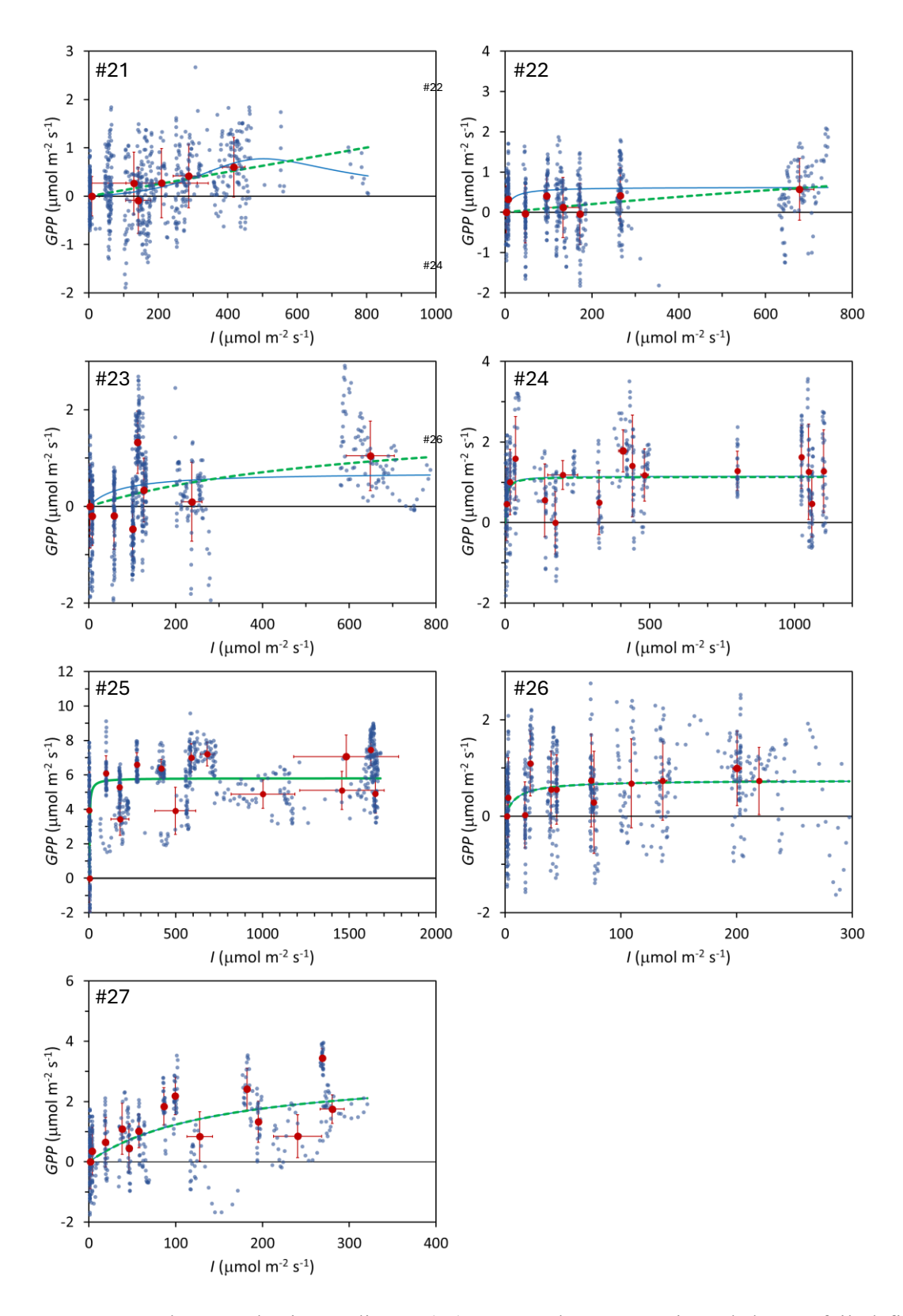


Figure S3: Photosynthesis-Irradiance (PI) curves that were rejected due to failed fitting of the Monod and Bernard-Rémond models.